Quantum dots-labeled polymeric scaffolds for *in vivo* tracking of degradation and tissue formation

Kun Hee Sim [a], Seyed Mohammand Mir [b], Sophia Jelke [a], Solaiman Tarafder [a], Jinho Kim [b,**], Chang H. Lee [a,*]

[a] Regenerative Engineering Laboratory, Center for Dental and Craniofacial Research, Columbia University Irving Medical Center, 630 West 168th Street, VC12-211, New York, NY, 10032, USA
[b] Department of Biomedical Engineering, Stevens Institute of Technology, Hoboken, NJ, 07030, USA

ARTICLE INFO

ABSTRACT

The inevitable gap between *in vitro* and *in vivo* degradation rate of biomaterials has been a challenging factor in the optimal designing of scaffold's degradation to be balanced with new tissue formation. To enable non-/minimum-invasive tracking of *in vivo* scaffold degradation, chemical modifications have been applied to label polymers with fluorescent dyes. However, the previous approaches may have limited expandability due to complicated synthesis processes. Here, we introduce a simple and efficient method to fluorescence labeling of polymeric scaffolds via blending with near-infrared (NIR) quantum dots (QDs), semiconductor nanocrystals with superior optical properties. QDs-labeled, 3D-printed PCL scaffolds showed promising efficiency and reliability in quantitative measurement of degradation using a custom-built fiber-optic imaging modality. Furthermore, QDs-PCL scaffolds showed neither cytotoxicity nor secondary labeling of adjacent cells. QDs-PCL scaffolds also supported the engineering of fibrous, cartilaginous, and osteogenic tissues from mesenchymal stem/progenitor cells (MSCs). In addition, QDs-PCL enabled a distinction between newly forming tissue and the remaining mass of scaffolds through multi-channel imaging. Thus, our findings suggest a simple and efficient QDs-labeling of PCL scaffolds and minimally invasive imaging modality that shows significant potential to enable *in vivo* tracking of scaffold degradation as well as new tissue formation.

1. Introduction

Various biomaterials have been widely applied for musculoskeletal tissue repair and regeneration, either as delivery carriers, grafts, or scaffolds [1–5]. The biomaterial-based carriers and scaffolds for tissue repair and regeneration are primarily biodegradable, as designed to allow a controlled release of bioactive factors or a balanced tissue formation replacing the scaffolds over time [1–7]. However, the mode and mechanism of biodegradation vary as associated with the chemical composition and physical configuration of each biomaterial-based structure [5,8,9]. Although some special biomaterial constructs are designed for active degradation in response to specific *in vivo* biochemical/physical environment at a target site [10], the most commonly used, polyester-based scaffold materials such as polycaprolactone (PCL),

poly (L-lactic acid) (PLLA), poly (glycolic acid) (PGA), and poly (lactic-co-glycolic acid) (PLGA) undergo passive degradation, primarily hydrolysis [11]. As biomaterial scaffolds are required to provide structural support at the implantation site until new tissue is formed and matured with functional restoration, the degradation rate of scaffolds is an essential factor to be considered for successful tissue regeneration *in vivo*.

The degradation rates of widely used polyester-based material scaffolds have been well characterized. However, the degradation tests have been limitedly conducted under controlled *in vitro* settings. Degradation of scaffolds is not only regulated by passive hydrolysis but also by mechanical and biochemical factors *in vivo* [11]. For example, enzymatic activities and cell-mediated breakdown are closely involved with *in vivo* scaffold degradation [11]. From our years of investigations in

---

Peer review under responsibility of KeAi Communications Co., Ltd.

* Corresponding author. Center for Dental and Craniofacial Research, Columbia University Irving Medical Center, 630 West 168th street, VC12B, New York, NY 10032, USA.
** Corresponding author.
E-mail addresses: jkim6@stevens.edu (J. Kim), chl2109@cumc.columbia.edu (C.H. Lee).

scaffold-based tissue regeneration, we have learned that the same type of scaffold can degrade at significantly different rates depending on animal species and implantation location [1–4,12–14]. Thus, there is an inevitable gap in scaffold degradation rates between *in vitro* and *in vivo* [15,16]. To track *in vivo* degradation of scaffolds, fluorescence labeling of scaffold materials has been applied [17–19]. For example, an organic fluorophore, di(thiophene-2-yl)-diketopyrrolopyrrole (DPP), was covalently linked in PCL that resulted in yellow fluorescence [17]. Similarly, other fluorescent dyes in blue, green, red, and near-infrared (NIR) have been linked with PCL via covalent bonding to synthesize PCL-dye-PCL [17]. In another study, NIR fluorophore-conjugated copolymer of PCL, PLLA, and PGA was synthesized for bone tissue engineering scaffold [19]. NIR signal at 800 nm emitted from the scaffold showed promising efficiency of tracing *in vivo* scaffold degradation [19]. Despite the promising outcome of the existing fluorescent polymers for *in vivo* tracking of degradation, the synthesis of fluorophore-conjugated materials requires complicated processes and unique facilities for quality control of the chemical reactions [17–19]. Moreover, a specific chemical modification needs to be implemented for optimal labeling for each biomaterial, consequently serving as a barrier for expanded applications.

This study introduces a simple and straightforward method to label a wide range of biomaterials using quantum dots (QDs), nanometer-sized fluorescent semiconductor crystals [20–22]. QDs have a tunable band gap ranging from the visible to the infrared (IR), high quantum yields (QYs), narrow and symmetric emission features, broad absorption above the band gap, large multiphoton absorption cross-sections, and high photostability [21–23]. These unique optical properties of QDs have been considered ideal for *in vivo* imaging [21,22]. Similarly, QDs have been extensively utilized for labeling cells, micelles, controlled delivery vehicles, cancer-targeting probes, and scaffolds for long-term tracking and deep-tissue imaging in live animals [21,24,25]. Here we adopted QDs with NIR light emission. Fluorescence in NIR wavelength (700–1000 nm) is suitable for deep-tissue *in vivo* imaging given its superior tissue penetration capacity and minimal interference with adjacent tissues to those of visible light [23,26]. We successfully fabricated a 3D-printed PCL scaffold labeled with NIR QDs that exhibited a promising potential for minimal- or non-invasive imaging and quantification of degradation as well as new tissue formation. We show a promising potential of imaging the QD-labeled PCL via an optical fiber inserted into tissue that enables to apply an excitation light directly to deep-tissue implanted scaffolds and to acquire the emission light traveling through the optical fibers. The fiber-optic imaging modality allowed us to achieve minimally invasive imaging regardless of the tissue thickness. This study may suggest a reliable and straightforward method to label polymeric scaffolds for *in vivo* tracking of degradation to be balanced with tissue healing.

2. Materials and methods

2.1. QD labeling of PCL

We labeled PCL with QDs via a physical composition, not through a chemical reaction or affinity binding. Briefly, Green CdSe QDs (excitation/emission: 500 nm/505–530 nm) and NIR CuInS/ZnS QDs (488 nm/700–800 nm) were purchased from NNCrystals (Fayetteville, AR). We first precipitated QDs from the reaction mixture by adding methanol and chloroform, followed by isolation via centrifugation as previously described [24]. The isolated QDs were redissolved in a 6:1 solvent mixture of chloroform and dimethylformamide (DMF) (Sigma-Aldrich, St. Louis, MO). Then GMP-grade PCL (PURASORB® PC 12; 1.0–1.3 dl/g; Corbion, Palatine, IL) was dissolved in the QD-solvents at 15 wt%, followed by vigorous stirring overnight. The final concentration of QDs was prepared at 0.3–0.5 wt% of PCL. The prepared PCL slurry was vacuum-dried for 48 h, and its fluorescence was confirmed using fluorescence microscopy with a FITC filter.

2.2. Fabrication and imaging of QDs-labeled PCL scaffold

The QDs-PCL was fabricated into scaffolds in a dimension of 5 mm × 5 mm x 1.5 mm using 3D Bioplotter® (4th generation, EnvisionTEC, Germany) as per our well-established methods [1,2,4]. Briefly, the prepared QDs-PCL was loaded in a high-temperature dispensing cartridge of Bioplotter® and heated up to 120 °C. The material was then dispensed through a stainless-steel needle to build 3D structures consisting of 400 μm micro-strands and 200 μm inter-strand channels. For initial imaging to confirm fluorescence, Maestro™ *in vivo* imaging system (Caliper Life Science, Waltham, MA) was utilized by applying a spectrum of excitation light (400–600 nm wavelength) on top of scaffolds. The emission signals were acquired by a top-positioned CCD camera at 515 nm and 780 nm for green and NIR QDs, respectively. To determine the feasibility of *in vivo* imaging, the NIR QDs-PCL scaffolds were implanted in the knee joint of Sprague-Dawley rat cadavers, followed by imaging with Maestro™ at 488 nm/780 nm. To measure tissue thickness allowing non-invasive deep-tissue imaging of scaffolds, we imaged QD-PCL scaffolds placed under multiple layers of rat skins up to 3 mm thickness.

2.3. Fiber-optic imaging set-up

Although QDs' emission at the NIR range is suitable for deep-tissue penetration with minimal tissue interference, the excitation light at a short wavelength is largely blocked by tissue barriers [23]. This may serve as a challenge in achieving sufficient excitation from the light applied on top of tissue layers to the scaffold embedded under thick tissues. To further enhance *the in vivo* imaging quality of the QDs-PCL scaffolds embedded in tissue layers, we built a custom-designed imaging system implemented with optical fibers and probe as in our previous works [27]. Briefly, our imaging system was designed to illuminate 488-nm laser light directly onto the scaffold through an optical probe, as 780-nm emission light from the target materials is collected by a CCD camera located on the overlaid tissue surface or through the same probe simultaneously. We used optical fibers of 700–1000 μm in diameter, allowing minimally invasive insertion inside tissues. Imaging probes consisted of A GRIN lens (LRL-070-P300, Oroton) and an optical-fiber imaging bundle (FIGH-03-215S, Fujikura) integrated into the epi-illumination compartment of the custom-built fluorescent imaging microscope. The laser light sheet was created by passing the laser beam (Jive 200 mW laser, Cobolt) through a cylindrical lens (ACY254-050-A, Thorlabs). Fluorescent signals from fluorescent QDs (780 nm) were separated from the excitation light (488 nm) by using a dichroic mirror (FF596-Di01-25 × 36, Semrock). The separated emission light signals were passed through an optical filter (FF02-641/75-25, Semrock) and detected by a camera (Zyla sCMOS 4.2, Andor) with the 10 × (PlanN 10 × , NA 0.25, Olympus) objectives. The obtained image data were processed using a custom-built algorithm based on the Fourier transform to remove structural and background noise from the images as per our prior works [27].

2.4. Accelerated in vitro degradation of QDs-PCL scaffolds

To determine a statistical correlation between the scaffold degradation and quantitative intensity of fluorescent signals, the QDs-PCL scaffolds (10 mm × 10 mm x 5 mm) underwent accelerated *in vitro* degradation by 1 M NaOH treatment, along with imaging by the custom-built optical-fiber system. Up to 38 days, the degradation of scaffolds was quantified by loss of dry weight and compressive moduli, measured at 0.1% strain/sec using UniVert mechanical tester (CellScale Biomaterials Testing, Waterloo, ON, Canada) as per our well-established protocols [2,4] (n = 5 per group and time point). PCL scaffolds without QDs labeling were tested as controls. The signal intensities at 780 nm were quantified using our own custom-built digital imaging processing [27]. Spearman's correlation test analyzed a statistical

correlation between degradation and deep-tissue fluorescence intensity [28].

2.5. Cytotoxicity of QDs-PCL

Cytotoxicity of QDs-labeled PCL scaffolds was measured using Transwell® co-culture with P1-2 human bone marrow-derived mesenchymal stem/progenitor cells (MSCs) (All Cells, Alameda, CA). Briefly, QDs-PCL scaffolds, after undergoing seven days of *in vitro* accelerated degradation, were placed on Transwell® inserts where MSCs were monolayer-cultured on the bottom substrate. Controls included groups with no scaffold and PCL scaffolds without QDs. The numbers of live cells were then counted for six days culture in growth media. Fluorescence microscopy was used at 1, 2, 3, and 6 days of culture to identify any QDs cleaved from scaffolds on the MSC culture plate.

2.6. Multi-lineage differentiation of MSCs in 3D-printed QDs-PCL scaffolds

To test tissue formation in the QDs-PCL scaffolds, P2-3 MSCs (2×10^6/ml) were seeded via collagen gel as per our prior works [2,13]. Briefly, cells were suspended in neutralized type I collagen solution, infused into scaffold's microchannels, and then incubated for 1 h at 37 °C for gelation. PCL scaffolds without QDs were used as control. The cell-seeded scaffolds were cultured for four weeks in fibrogenic, chondrogenic, and osteogenic differentiation media as per our previous studies [1,2,4,13,29]. Fibrogenic differentiation supplements included 100 ng/ml connective tissue growth factor (CTGF) (BioVendor, Candler, NC) and 50 μg/ml ascorbic acids. The chondrogenic medium was supplemented with 10 ng/ml transforming growth factor β3 (TGFβ3) (R&D Systems, Minneapolis, MN), whereas the osteogenic medium was supplemented with 100 nM dexamethasone, 10 mM β-glycerophosphate, and 0.05 mM ascorbic acid-2-phosphate (Sigma) per our prior methods [1,2,4,13,29]. At four weeks, all samples were harvested for histological analysis. Randomly selected 5-μm thick tissue sections were stained with H&E, picrosirius red (PR) (staining for collagen), safranin O/fast green (Saf-O/FG) (staining for cartilaginous matrix), and alizarin red (AR) (staining for Ca^{2+}-rich mineralized matrix). Fluorescence microscopy was used to image FITC (519 nm) and NIR signals (780 nm) from the engineered tissues in PCL and QDs-PCL scaffolds cultured with MSCs. In addition, digital imaging processing was performed to quantify fluorescent signal intensity as per our prior studies [12,27].

2.7. Statistical analysis

For all the quantitative data, following confirmation of normal data distribution, one-way analysis of variance (ANOVA) with post-hoc Tukey HSD tests were used with a p-value of 0.05. Sample sizes for all quantitative data were determined by power analysis with one-way ANOVA using a level of 0.05, power of 0.8, and effect size of 1.50 chosen.

3. Results

3.1. Fluorescent PCL blended with QDs

We have successfully established a simple protocol for the efficient labeling of PCL scaffolds. Mixture with QDs at 0.3 wt% and 0.5 wt% resulted in a solid fluorescent signal at 520 nm emission (Fig. 1A). The 3D-printed scaffolds labeled with green QDs and NIR QDs showed strong emission at respective wavelengths compared to no emission from PCL scaffolds without QDs (Fig. 1B). Application of excitation light over tissue layers by Maestro™ system (Fig. 1C) showed NIR signals from scaffolds implanted in the rat knee joint (Fig. 1D). However, the overlaid animal tissues diminished the intensity of NIR emission signals detected through tissue layers (Fig. 1E).

3.2. Fiber-optic imaging to improve deep-tissue detection

We designed a fiber-optic imaging modality that allows detection of NIR emission both on the overlaid tissue surface and through an optical probe inserted inside the tissues (Fig. 2A). A custom-built image system
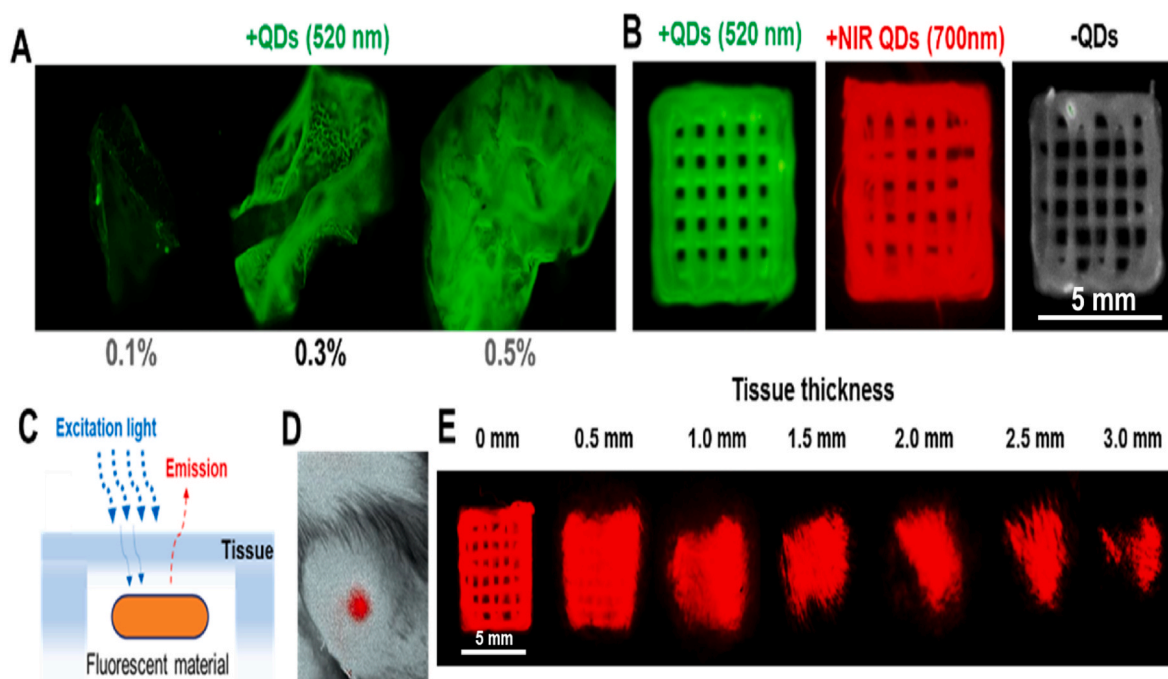

Fig. 1. A mixture of QDs >0.3 wt% showed strong fluorescence (**A**), and QD-labeled PCL was successfully 3D-printed (**B**). Application of excitation light over tissue layers (**C**) successfully detected QDs-PCL scaffolds implanted in the rat knee joint (**B**). However, the NIR signal intensity gradually decreased with the increasing thickness of overlaid tissues (**E**), suggesting the limitation of QD excitation through tissue layers.
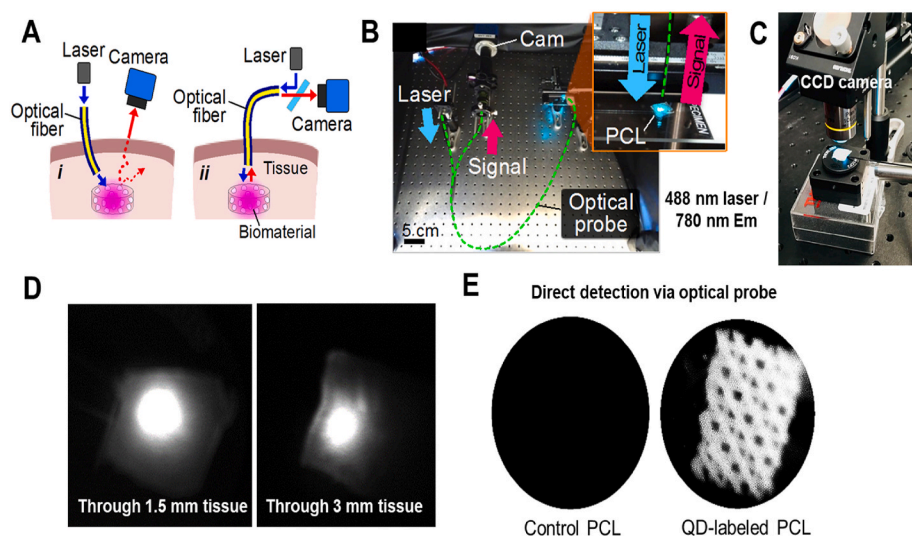
Fig. 2. An optical fiber-imaging system was designed to directly illuminate implanted scaffolds and imaging of emission (**A**). The hardware set-up of the imaging system (**B**) shows optical fibers connecting probe, light source, and a CCD camera (**C**). Excitation through optical fibers inserted into tissue layers resulted in the successful detection of emission light through the tissue layers (**D**). Direct emission detection via inserted optical probe also showed strong signal from QDs-labeled PCL scaffolds in contract to control PCL without QD (**E**).

comprises flexible optical fiber connecting the laser source to the optical probe connected back to a camera (Fig. 2B). A separate CCD camera was installed for signal detection on the tissue surface (Fig. 2C). When QDs-PCL scaffolds were imaged under animal tissue, the CCD camera acquired strong NIR signals, both with 1.5 mm and 3.0 mm thick tissue cover (Fig. 2D). In addition, a strong NIR signal from the QDs-PCL scaffold was detected via the optical probe inserted through the tissue cover in contrast to no signal from the PCL scaffold (Fig. 2E). The direct detection via an optical probe, as emission light travels through the inserted optical fiber to the camera at the other end, has no signal interference regardless of the thickness of tissue layers. This is consistent with our previous study that demonstrated a robust imaging efficacy of labeled cells inside animal's lung using the fiber-optic imaging system [27].

3.3. Degradation of QDs-PCL scaffolds correlated with fluorescence intensity

Macroscopically, PCL and QDs-PCL treated with 1 M NaOH up to 38 days showed structural breakdown with significant enlargement of pores (Fig. 3A). Quantitatively, the percent of degradation calculated by remaining dry weights increased over time by 38 days both in PCL and QDs-PCL (Fig. 3B). Consistently, the compressive moduli of both PCL and QDs-PCL scaffolds gradually decreased over time (Fig. 3C). The weight loss and compressive moduli suggested that QDs-PCL exhibit a faster degradation rate than PCL (Fig. 3B and C) (n = 5 per group; p < 0.01). The NIR images acquired by our fiber-optic imaging system consistently showed a gradual decrease in the signal intensity for 38

days (Fig. 4A). Quantitative light intensity at 780 nm wavelength also showed declines over time (Fig. 4B). Spearman's correlation test demonstrated a statistically significant disproportional correlation (R = −0.981) between the degradation rate and fluorescent signal intensity (Fig. 4C) (n = 8–10 per time point; p < 0.000001), suggesting the NIR signal detected through the optical probe is a reliable indicator of scaffold degradation.

3.4. No observed cytotoxicity of QDs-PCL scaffolds

Transwell® co-culturing of degrading QDs-PCL scaffolds with MSCs (Fig. 5A) showed no sign of any cytotoxicity up to 6 days culture, given the increasing number of live cells over time with no statistically significant difference from no scaffold control and PCL control (Fig. 5B) (n = 5 per group). Furthermore, fluorescence image overlapped with brightfield microscopic image identified very few spotty clusters of cleaved QDs during the PCL degradation (Fig. 5C). Nonetheless, the cleaved QDs appeared not to be taken up by adjacent cells (Fig. 5C).

3.5. In vitro tissue formation in QDs-PCL scaffolds

After 4 weeks of culture in respective differentiation media, both PCL and QDs-PCL scaffolds seeded with MSCs formed dense tissue matrix as compared to control cultured in growth media, with no noticeable difference between PCL and QDs-PCL scaffolds (Fig. 6A). Specific staining further suggested that PCL and QDs-PCL are suitable for guiding MSC's differentiation into the selected tissue types (Fig. 6B–D). PR staining showed dense fibrous tissue matrix formed both in PCL and QDs-PCL
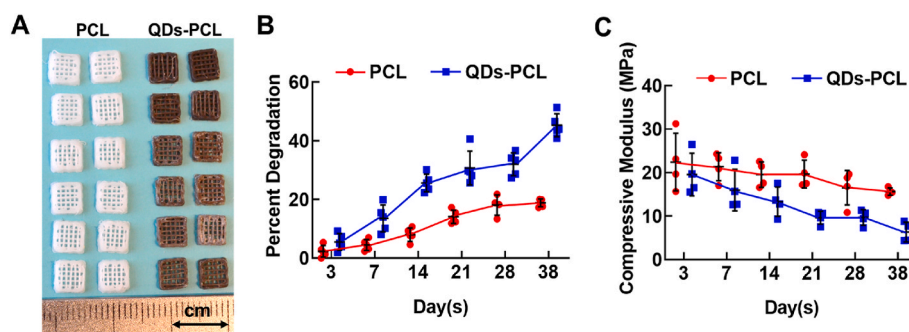

Fig. 3. In vitro accelerated degradation of 3D-printed PCL and QDs-PCL scaffolds. Both PCL and QDs-PCL scaffolds showed structural breakdown by 1 N NaOH treatment for 38 days (**A**). Percent of degradation measured by dry weight loss (**B**) and compressive moduli (**C**) consistently showed a gradual decrease over time, with somewhat slowed degradation of QDs-PCL as compared to PCL (n = 6 per group and time point).
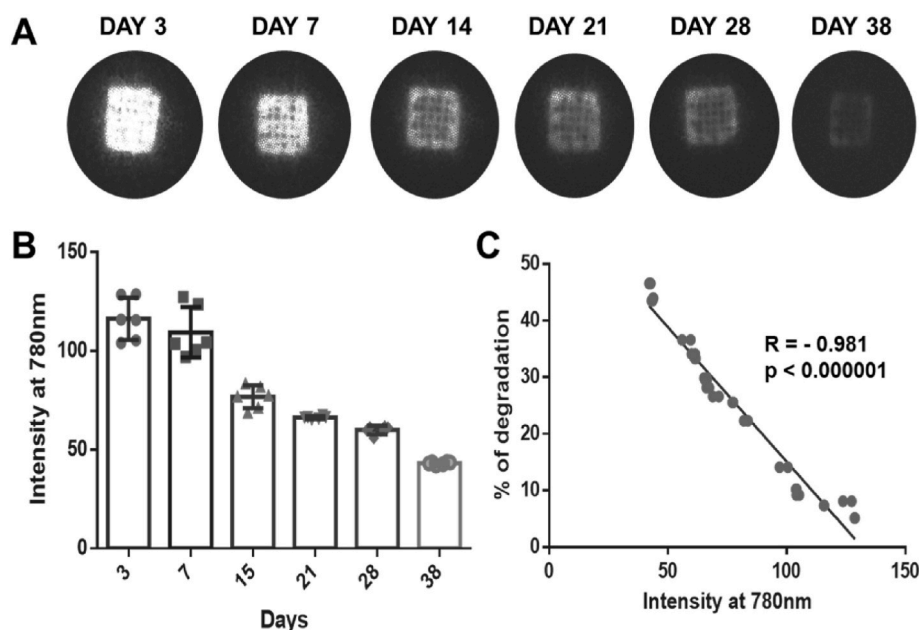
Fig. 4. Correlation between NIR signal intensity and scaffold degradation. Degrading QDs-PCL scaffolds showed decreased NIR signal intensity over time (A). Quantitatively, the signal intensity was reduced over time (**B**) that were statistically correlated with the percent of degradation (**C**) (n = 10–15 per time point).
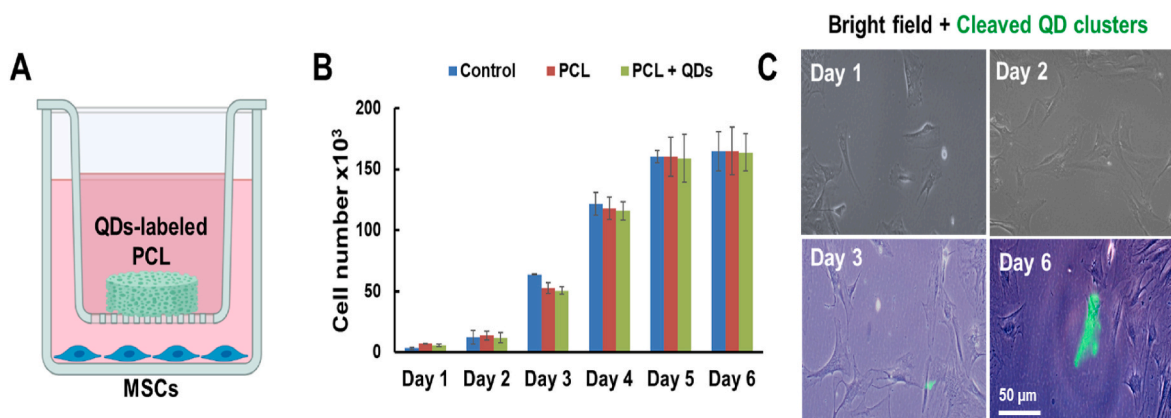

Fig. 5. Co-culture of QDs-PCL scaffolds with MSCs (A) showed no sign of cytotoxicity demonstrated by no difference in live cell number for six days compared to controls with no scaffold and PCL alone (**B**). In addition, fluorescence microscopy identified a few spotty cleaved QDs starting 3 days, but no sign of secondary labeling was observed (**C**).

compared to control without fibrogenic differentiation media (Fig. 6B). Saf-O/FG staining showed cartilaginous matrix formation in PCL and QDs-PCL scaffolds seeded with MSCs (Fig. 6C). Similarly, AR staining showed a mineralized tissue matrix in PCL and QDs-PCL scaffolds (Fig. 6D). These findings suggest that QD labeling has no negative effect on the capability of PCL scaffold in support of multi-lineage tissue formation. Under observation with FITC (495 nm/519 nm), QDs-PCL showed no autofluorescence, unlike the strong autofluorescence from unlabeled PCL scaffolds (Fig. 7A). In addition, the MSC-derived multiple types of tissue matrix showed notable autofluorescence (Fig. 7A) with some degree of tissue type-dependent intensity (Fig. 7B). Given the lack of autofluorescence of QDs-PCL and strong autofluorescence of *de novo* tissues, multi-channeled fluorescence with FITC (519 nm) and NIR (780 nm) clearly distinguished the remaining structure of QDs-PCL scaffolds from newly formed tissue matrix (Fig. 7C). The autofluorescence-based detection of newly forming tissues was challenging due to the autofluorescence of PCL at the same excitation and emission (Fig. 7C). These observations may suggest the potential of QDs-PCL scaffold for *in vivo* tracking of scaffold degradation and new tissue formation.

4. Discussion

Our findings suggest a simple and efficient QDs-labeling of PCL scaffolds and minimally invasive imaging modality that may have the potential to enable *in vivo* tracking of scaffold degradation and new tissue formation. QDs are semiconductor nanometer-sized crystals with unique photochemical and photophysical properties, such as improved brightness, lacked photobleaching, and multicolor fluorescence emission. Furthermore, unlike the previous methods involved with chemical modifications and reactions, our QDs-based labeling is a simple process any lab can easily use and is applicable for various materials such as synthetic polymers, natural and synthetic hydrogels, and bioadhesive.

Since QDs have been widely utilized for *in vivo* tracking of labeled cells, we performed *an in vitro* co-culture experiment to ensure no secondary labeling of QDs cleaved from degrading scaffolds. Our data strongly suggest that QDs-blended in PCL scaffolds provide accurate imaging of scaffolds without labeling adjacent cells/tissue. Few previous studies performed a passive QD labeling of cells where QDs undergo endocytosis as being incubated with cells for a prolonged duration [30].
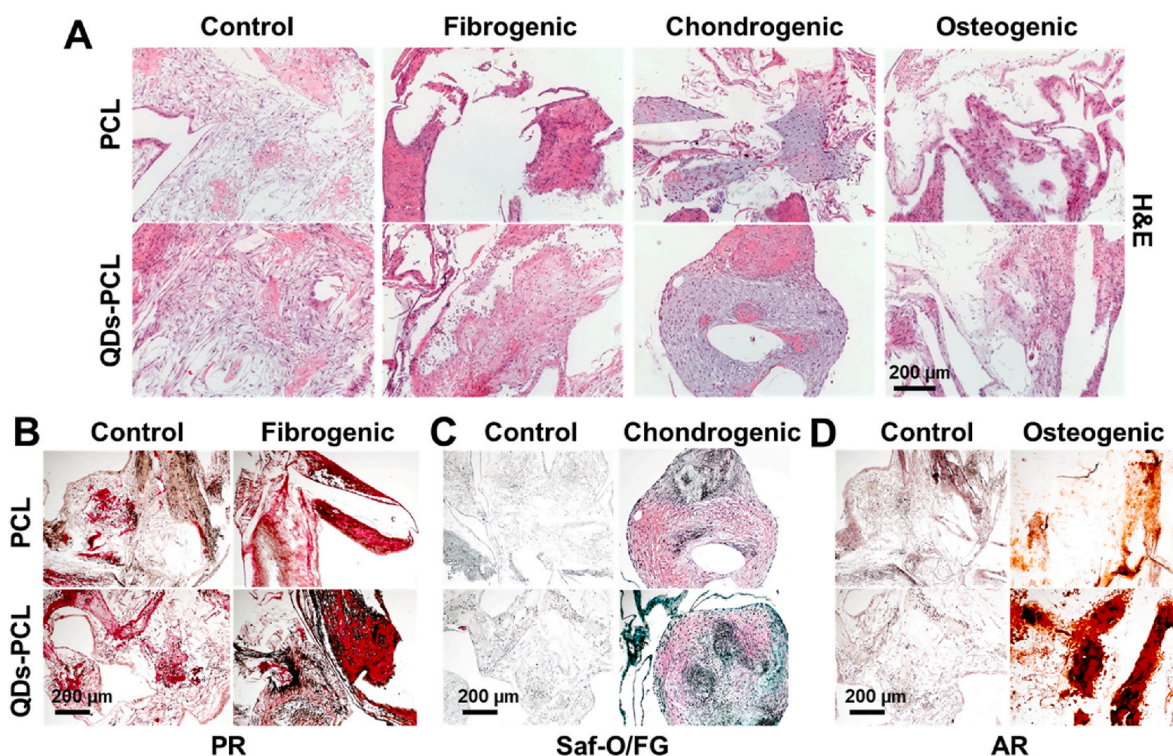
Fig. 6. Differentiation of MSCs seeded on QDs-PCL scaffolds to fibrogenic, chondrogenic, and osteogenic lineages for 4 weeks *in vitro*. H&E sections (**A**) showed dense tissue matrix formed under respective differentiation media, with no noticeable difference between PCL and QDs-PCL scaffold. PR (**B**), Saf-O/FG (**C**), and AR (**D**) staining showed fibrous, cartilaginous, and mineralized tissue formation, respectively, without notable difference between PCL and QDs-PCL scaffolds.
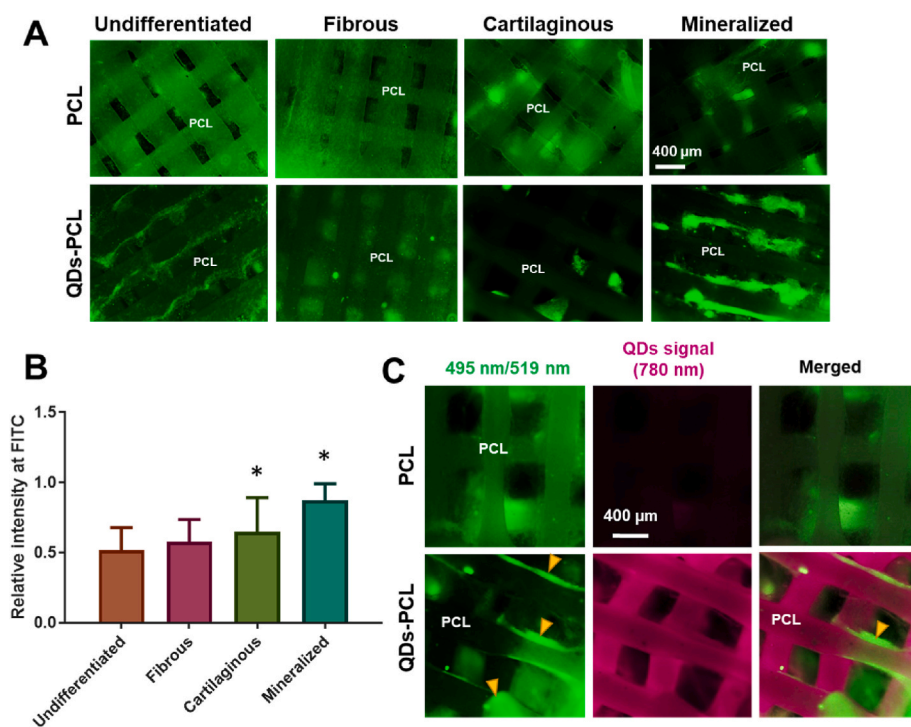

Fig. 7. Multi-channel fluorescence microscopy showed that autofluorescence of PCL at 495nm/519 nm disappeared by QD labeling, while autofluorescence of newly forming tissue matrix is visible (**A**). The intensity of autofluorescence of newly forming tissues varied depending on the type of tissues (**B**) (*:$p < 0.005$ compared to undifferentiated control; $n = 10$ per group). In contrast to PCL scaffolds showing green autofluorescence as same as tissue autofluorescence, QDs-PCL allowed distinguishing the green tissue autofluorescence from the remaining scaffolds detected at 780 nm emission (**C**) (arrows indicate newly forming tissues). (For interpretation of the references to color in this figure legend, the reader is referred to the Web version of this article.)

However, QD-labeling of cells has been dominantly performed by active labeling with surface functionalization of QDs to target specific cells [21, 22,25]. Accordingly, it is postulated that QDs in this study, physically blended in PCL without any functionalization, possess a low possibility to undergo endocytosis into adjacent cells. Besides, the slow degradation of PCL limiting the amount of QD cleavage at given times and the versatile *in vivo* environment with fluid flow and diffusion may further lower the possibility of secondary QD-labeling *in vivo*.

Despite the unique optical properties of QDs, the potential cytotoxicity of QDs has been an unresolved issue for their preclinical

applications [31]. Although a recent primate study showed no cytotoxicity of *in vivo* injected QDs [32], it is worth fully considering the potential cytotoxicity of QDs to be delivered with slow degrading PCL scaffolds. It has been suggested that QD cytotoxicity is associated with the physiochemical properties, as connected with some inherent chemical feature such as the elements contained in the QD core [31,33]. Some studies have suggested that the elemental toxicity is mainly dependent upon the accessibility of the core atoms to the surrounding solvent [31,34]. In addition, previous studies showed a meaningful correlation between QD cytotoxicity and Cd^{2+} release and its cellular uptake [20,31]. Another study suggested that surface oxidation of QDs leads to the release of free cadmium ions, resulting in apoptosis [20]. Thus, no QD cytotoxicity shown in this study is potentially attributed to the low QD amount (0.3 wt%), the limited endocytosis, and the adoption of CuInS/ZnS free of cadmium. Consistently, a previous study showed no cytotoxicity of unfunctionalized CuInS/ZnS QDs in contrast to Cd-based QDs [35]. Despite the paucity of *in vivo* outcome, the major weakness of this study, the *in vitro* cytotoxicity data strongly advocate the *in vivo* safety of our QD-PCL scaffolds considering the small QD dose per scaffold, the slow *in vivo* degradation rate resulting in negligible amount of QD cleavages at a certain time-point, and the quick *in vivo* QD diffusion rate (<2 h) reported in literature [36].

An interesting observation in this study is that QDs-labeling minimized green-light autofluorescence of PCL by darkening the color of PCL scaffolds (e.g., Fig. 3A). Despite being an unexpected finding with unknown mechanism, this feature was highly beneficial in distinguishing the mass of remaining scaffolds from those of newly forming tissues showing strong autofluorescence in green light. Furthermore, with multi-channeled fluorescence imaging for green and NIR wavelengths, we have demonstrated the feasibility of tracking scaffold degradation and the formation of new tissue. In conclusion, QDs-PCL scaffolds with optical-fiber imaging modality have significant potential in our efforts to optimize the degradation rate of biodegradable scaffolds as balanced with *in vivo* tissue regeneration. As scaffold degradation and rate of new tissue formation may vary between individual animals, species, and human patients, our study enabling minimally invasive *in vivo* tracking has significant implications in scaffold-supported tissue engineering and regenerative medicine.

Conflict of interest

All authors have no conflict of interest to disclose.

Data and materials availability

All the data presented in this study will be available upon request.

CRediT authorship contribution statement

Kun Hee Sim: was responsible for the primary technical undertaking and conducted the experiments. **Seyed Mohammand Mir:** performed construction and operation of the optical fiber-imaging system. **Sophia Jelke:** conducted preparation of QD-labeled PCL and initial imaging experiments. **Solaiman Tarafder:** performed in vitro MSC experiments and supported technical undertaking. **Jinho Kim:** Formal analysis, was responsible for the operation of optical fiber imaging and data analysis. **Chang H. Lee:** Formal analysis, is responsible for the study design, data analysis and interpretation, and manuscript preparation. All the authors edited the manuscript.

Declaration of competing interest

The authors declare that they have no known competing financial interests or personal relationships that could have appeared to influence the work reported in this paper.

References

[1] C.H. Lee, et al., Three-dimensional printed multiphase scaffolds for regeneration of periodontium complex, Tissue engineering, Part. Accel. 20 (7–8) (2014) 1342–1351.

[2] C.H. Lee, et al., Protein-releasing polymeric scaffolds induce fibrochondrocytic differentiation of endogenous cells for knee meniscus regeneration in sheep, Sci. Transl. Med. 6 (266) (2014), 266ra171.

[3] S. Tarafder, et al., Engineered healing of avascular meniscus tears by stem cell recruitment, Sci. Rep. 8 (1) (2018) 8150.

[4] S. Tarafder, et al., Micro-precise spatiotemporal delivery system embedded in 3D printing for complex tissue regeneration, Biofabrication 8 (2) (2016), 025003.

[5] J.M. Williams, et al., Bone tissue engineering using polycaprolactone scaffolds fabricated via selective laser sintering, Biomaterials 26 (23) (2005) 4817–4827.

[6] K. Legemate, et al., Engineering human TMJ discs with protein-releasing 3D-printed scaffolds, J. Dent. Res. 95 (7) (2016) 800–807, https://doi.org/10.1177/0022034516642404.

[7] M. Singh, et al., Microsphere-based seamless scaffolds containing macroscopic gradients of encapsulated factors for tissue engineering, Tissue Eng. C Methods 14 (4) (2008) 299–309.

[8] C.X. Lam, et al., Dynamics of in vitro polymer degradation of polycaprolactone-based scaffolds: accelerated versus simulated physiological conditions, Biomed. Mater. 3 (3) (2008), 034108.

[9] D.E. Perrin, J.P. English, Polycaprolactone, in: A.J. Domb, J. Kost, D.M. Wiseman (Eds.), Handbook of Biodegradable Polymers, Harwood Academic Publishers, Chur,Switzerland, 1997, pp. 63–77.

[10] M.I. Echeverria Molina, et al., Design Challenges in Polymeric Scaffolds for Tissue Engineering 9 (231) (2021).

[11] Y. Tokiwa, B.P. Calabia, Biodegradability and biodegradation of polyesters, J. Polym. Environ. 15 (4) (2007) 259–267.

[12] C.H. Lee, et al., Regeneration of the articular surface of the rabbit synovial joint by cell homing: a proof of concept study, Lancet 376 (9739) (2010) 440–448.

[13] C.H. Lee, et al., CTGF directs fibroblast differentiation from human mesenchymal stem/stromal cells and defines connective tissue healing in a rodent injury model, J. Clin. Invest. 120 (9) (2010) 3340–3349.

[14] Y. Nakagawa, et al., Long-term evaluation of meniscal tissue formation in 3-dimensional-Printed scaffolds with sequential release of connective tissue growth factor and TGF-beta 3 in an ovine model, Am. J. Sports Med. 47 (11) (2019) 2596–2607.

[15] Y. Cao, et al., The influence of architecture on degradation and tissue ingrowth into three-dimensional poly(lactic-co-glycolic acid) scaffolds in vitro and in vivo, Biomaterials 27 (14) (2006) 2854–2864.

[16] F. He, J. Ye, In Vitro Degradation, Biocompatibility, and in Vivo Osteogenesis of Poly(lactic-Co-Glycolic Acid)/calcium Phosphate Cement Scaffold with Unidirectional Lamellar Pore Structure, 100A, 2012, pp. 3239–3250, 12.

[17] S. Huang, et al., Highly Fluorescent Polycaprolactones with Tunable Light Emission Wavelengths across Visible to NIR Spectral Window 3 (17) (2016) 1600259.

[18] L. Jing, et al., Noninvasive in vivo imaging and monitoring of 3D-printed polycaprolactone scaffolds labeled with an NIR region II fluorescent dye, ACS Applied Bio Materials 4 (4) (2021) 3189–3202.

[19] S.H. Kim, et al., NIR fluorescence for monitoring in vivo scaffold degradation along with stem cell tracking in bone tissue engineering, Biomaterials 258 (2020) 120267.

[20] A.M. Derfus, et al., Probing the cytotoxicity of semiconductor quantum dots, Nano Lett. 4 (1) (2004) 11–18.

[21] H.-S. Han, et al., Quantum Dot/antibody Conjugates for in Vivo Cytometric Imaging in Mice, vol 112, 2015, pp. 1350–1355, 5.

[22] I.L. Medintz, et al., Quantum dot bioconjugates for imaging, labelling and sensing, Nat. Mater. 4 (6) (2005) 435–446.

[23] O.T. Bruns, et al., Next-generation in vivo optical imaging with short-wave infrared quantum dots, Nature Biomedical Engineering 1 (4) (2017), 0056.

[24] X. He, et al., Electrospun quantum dots/polymer composite porous fibers for turn-on fluorescent detection of lactate dehydrogenase, J. Mater. Chem. 22 (35) (2012) 18471–18478.

[25] K. Kikushima, et al., A non-invasive imaging for the in vivo tracking of high-speed vesicle transport in mouse neutrophils, Sci. Rep. 3 (1) (2013) 1913.

[26] G. Hong, et al., Near-infrared fluorophores for biomedical imaging, Nature Biomedical Engineering 1 (1) (2017), 0010.

[27] J. Kim, et al., Controlled delivery and minimally invasive imaging of stem cells in the lung, Sci. Rep. 7 (1) (2017) 13082.

[28] S. Gutman, et al., Regionally variant collagen alignment correlates with viscoelastic properties of the disc of the human temporomandibular joint, Arch. Oral Biol. 86 (2018) 1–6.

[29] C.H. Lee, et al., Tissue formation and vascularization in anatomically shaped human joint condyle ectopically in vivo, Tissue engineering, Part. Accel. 15 (12) (2009) 3923–3930.

[30] B.S. Shah, J.J. Mao, Labeling of mesenchymal stem cells with bioconjugated quantum dots, Methods Mol. Biol. 680 (2011) 61–75.

[31] S. Nikazar, et al., Revisiting the cytotoxicity of quantum dots: an in-depth overview, Biophysical Reviews 12 (3) (2020) 703–718.

[32] L. Ye, et al., A pilot study in non-human primates shows no adverse response to intravenous injection of quantum dots, Nat. Nanotechnol. 7 (7) (2012) 453–458.

[33] E. Oh, et al., Meta-analysis of cellular toxicity for cadmium-containing quantum dots, Nat. Nanotechnol. 11 (5) (2016) 479–486.

[34] C. Kirchner, et al., Cytotoxicity of colloidal CdSe and CdSe/ZnS nanoparticles, Nano Lett. 5 (2) (2005) 331–338.

[35] N. Tsolekile, et al., Cytotoxicity, fluorescence tagging and gene-expression study of CuInS/ZnS QDS - meso (hydroxyphenyl) porphyrin conjugate against human monocytic leukemia cells, Sci. Rep. 10 (1) (2020) 4936.

[36] K. Nekolla, et al., Influence of surface modifications on the spatiotemporal microdistribution of quantum dots in vivo, Small 12 (19) (2016) 2641–2651.